Electronic Supplementary Material (ESI) for Environmental Science: Processes & Impacts.

Supporting Information

A CFD Study on the Effect of Portable Air Cleaner Placement on Airborne Infection Control in a Classroom

Gen Pei[1], Parham Azimi[1], Donghyun Rim[2], Joseph G. Allen[1]*

[1] Environmental Health Department, Harvard T.H. Chan School of Public Health, Boston, MA 02115

[2] Architectural Engineering Department, Pennsylvania State University, University Park, PA 16802

*Corresponding author:

Gen Pei, Ph.D.

Tel: 1-814-852-9926

Email: gpei@hsph.harvard.edu

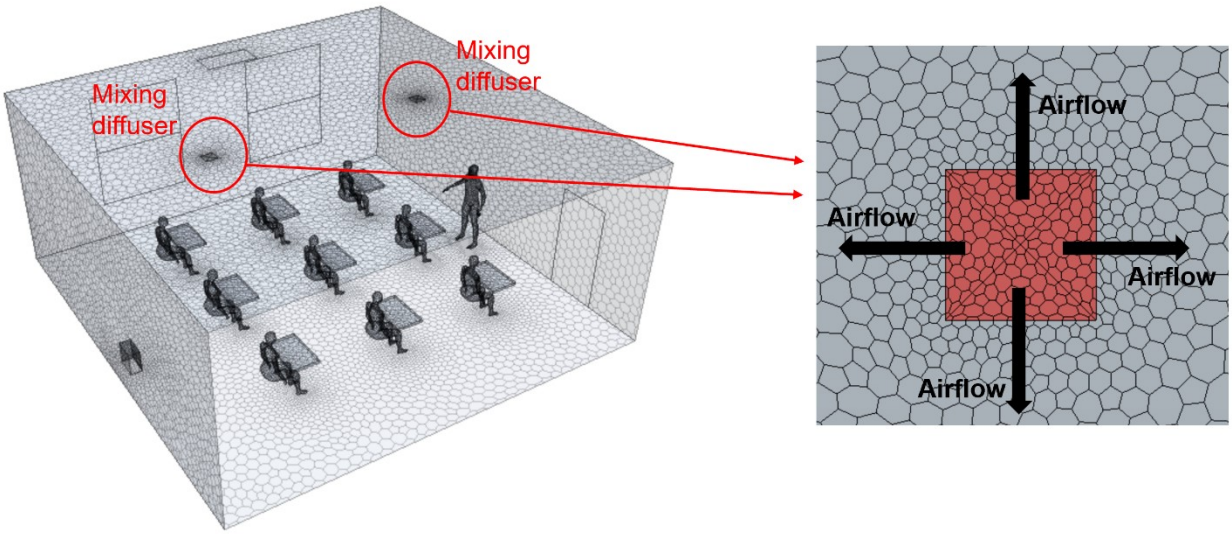

Figure S1. Description of four-way ceiling diffusers.

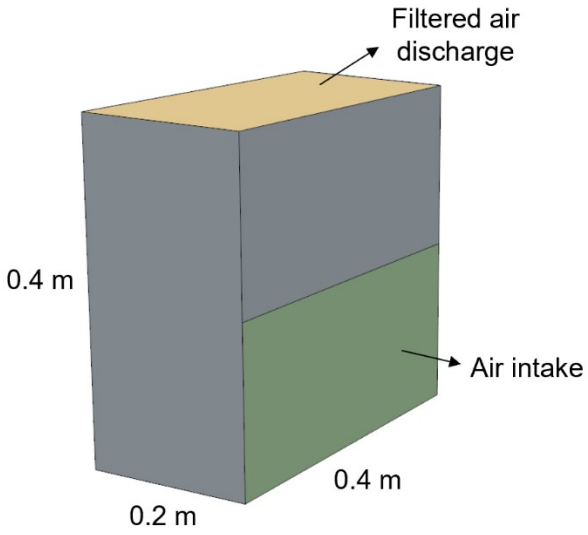

Figure S2. Illustration of modeled portable air cleaner.

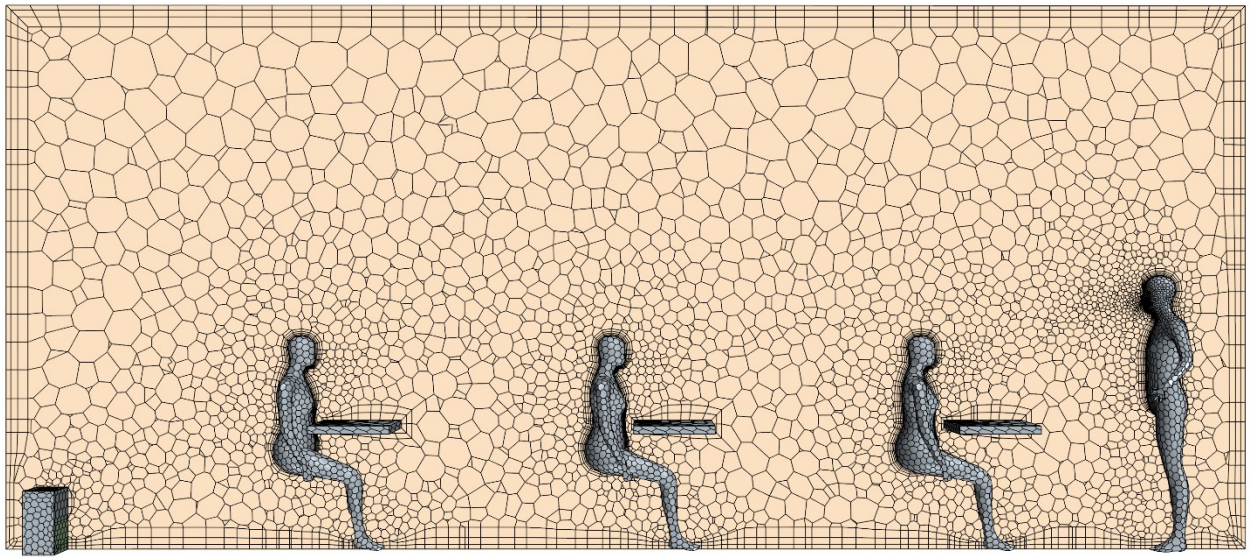

Figure S3. Details of computational grids near human bodies.

Table S1. Grid sensitivity analysis for three mesh strategies. Grid 2 is the adopted mesh in this study.

	Grid 1	Grid 2	Grid 3
Cell number	130,000	200,000	280,000
First cell size adjacent to human surfaces (m)	0.006	0.005	0.004
Human surface average y+	4.8	3.8	3.1
Breathing zone cell size (m)	0.06	0.05	0.04
Supply air diffuser: target cell size (m)	0.1	0.08	0.06
Supply air diffuser: minimum cell size (m)	0.05	0.04	0.03
Exhaust: target cell size (m)	0.1	0.08	0.06
Exhaust: minimum cell size (m)	0.05	0.04	0.02
Window: target cell size (m)	0.2	0.2	0.1
Window: minimum cell size (m)	0.1	0.05	0.04
PAC inlet: target cell size (m)	0.06	0.04	0.03
PAC inlet: minimum cell size (m)	0.02	0.02	0.02
PAC outlet: target cell size (m)	0.06	0.04	0.03
PAC outlet: minimum cell size (m)	0.02	0.02	0.02

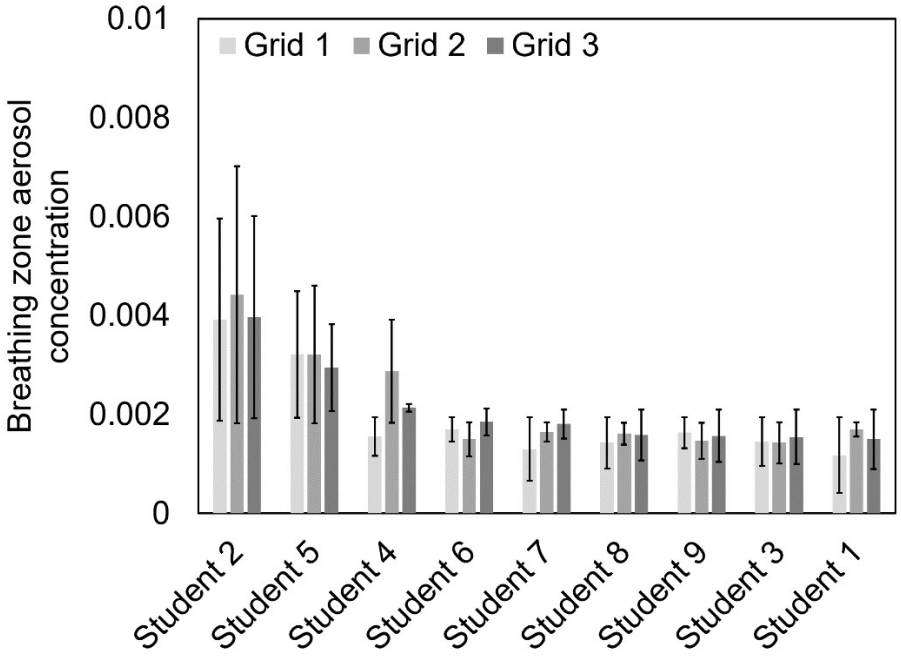

Figure S4. Breathing zone aerosol concentrations of nine students for three mesh strategies. The concentr ations are normalized by emission concentration. Error bars are standard deviations.

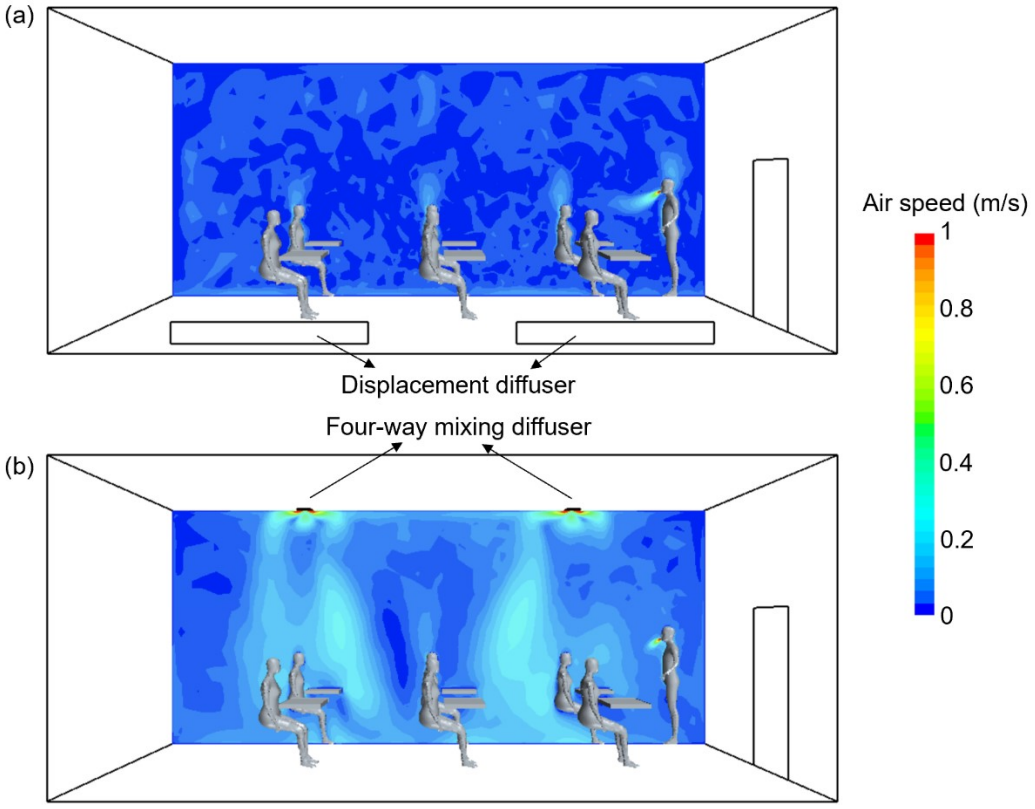

Figure S5. Contours of air speed under (a) displacement ventilation and (b) mixing ventilation. No portable air cleaner is applied.

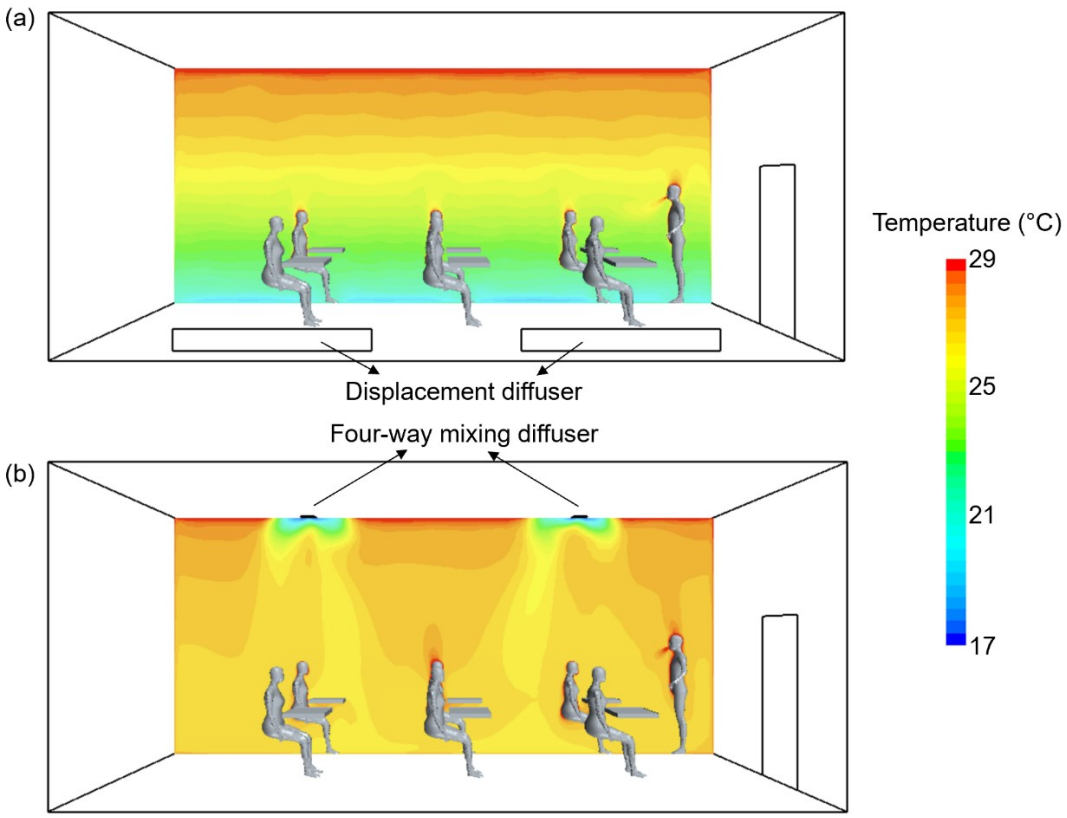

Figure S6. Contours of temperature under (a) displacement ventilation and (b) mixing ventilation. No portable air cleaner is applied.

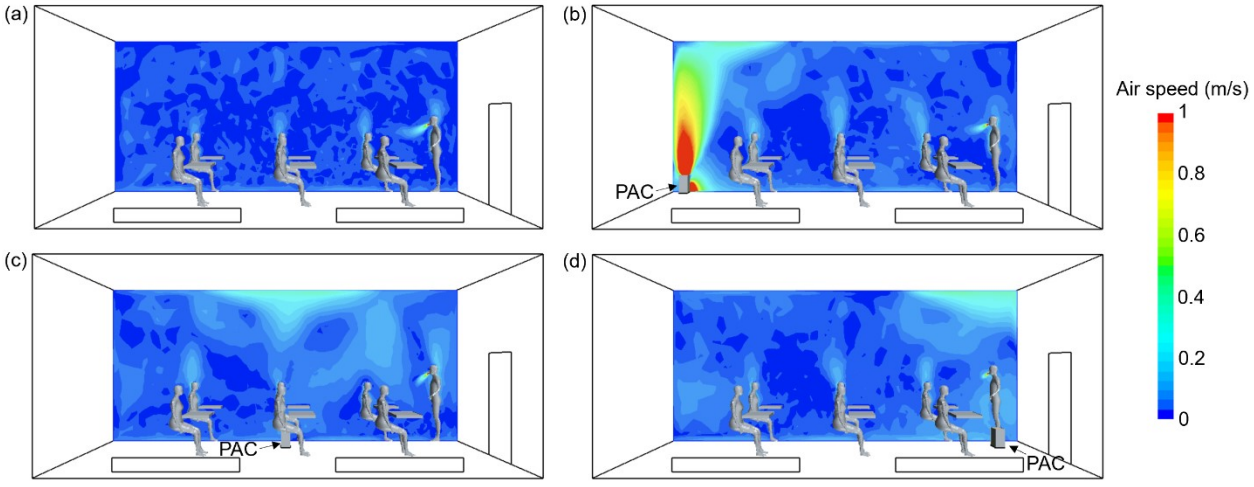

Figure S7. Contours of air speed under displacement ventilation. Four scenarios of deployment of portable air cleaner are shown: (a) without air cleaner, and with a single air cleaner at (b) 8 m, (c) 3 m, and (d) 0.5 m distance to the infector.

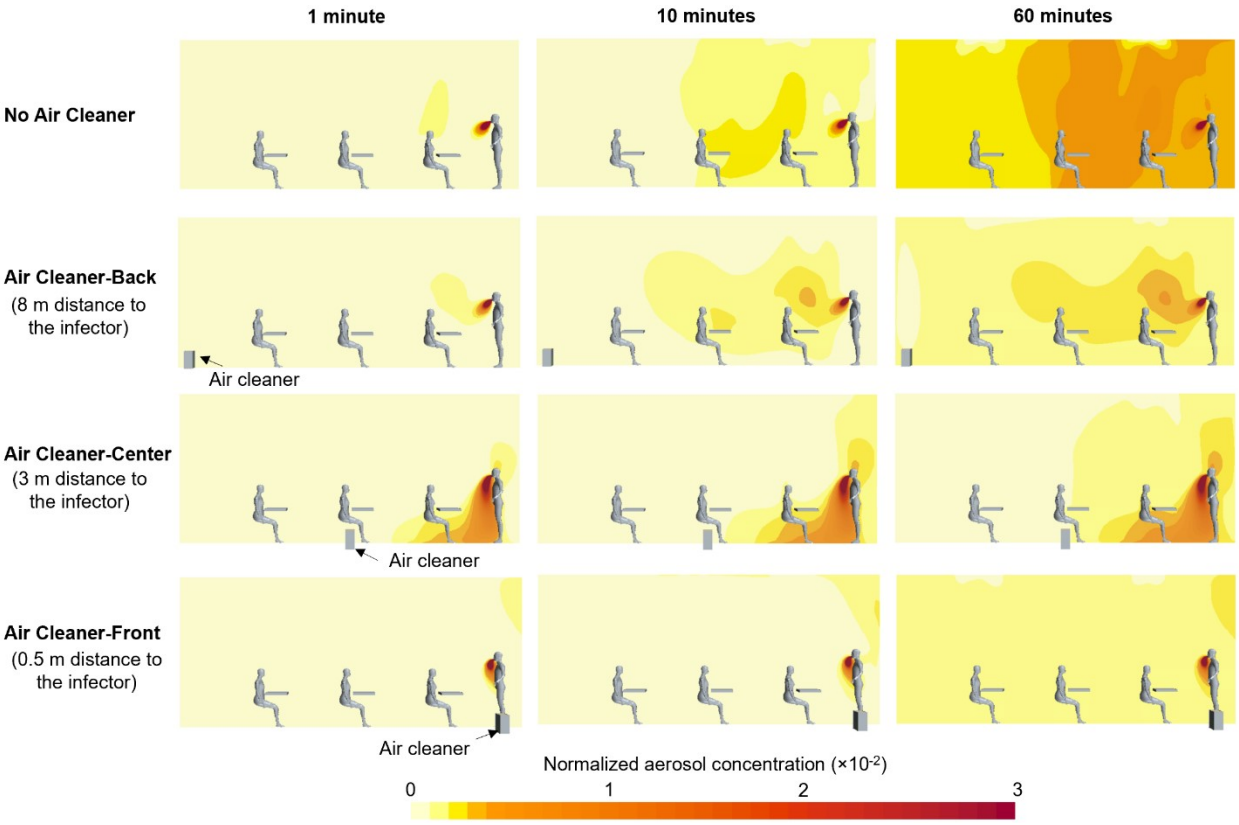

Figure S8. Temporal development of aerosol concentration distribution under mixing ventilation. Four scenarios of deployment of portable air cleaner are shown: without air cleaner and with a single air cleaner at 8 m, 3 m, and 0.5 m distance to the infector. The concentrations are normalized by emission concentration.

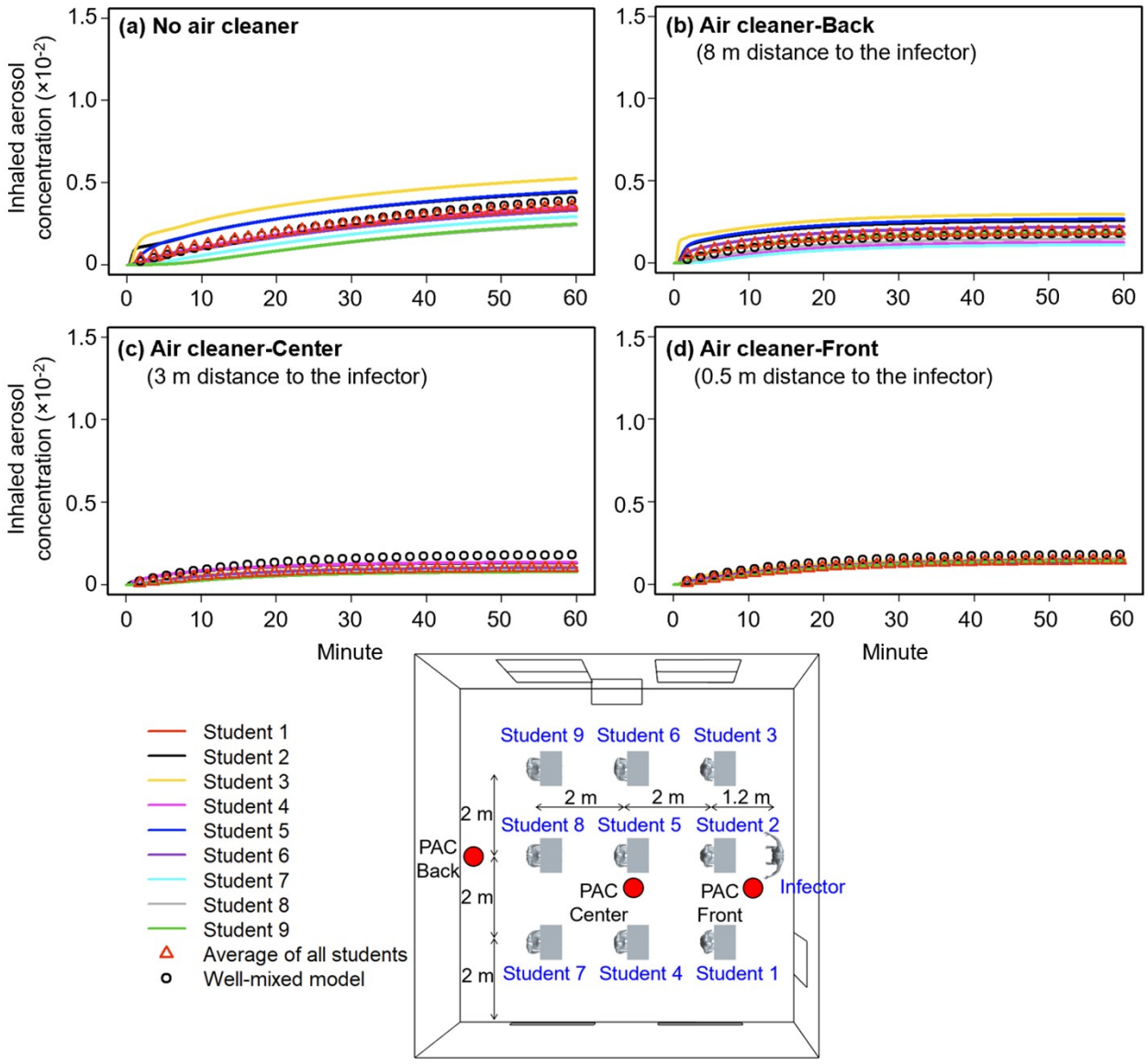

Figure S9. Transient inhaled aerosol concentration of nine students under mixing ventilation. Four scenarios of deployment of portable air cleaner are shown: (a) without air cleaner, and with a single air cleaner at (b) 8 m, (c) 3 m, and (d) 0.5 m distance to the infector. The simulation results are compared with the well-mixed mass balance model. The concentrations are normalized by emission concentration. PAC: portable air cleaner.

Supplementary Text S1. Experimental Validation

To validate our CFD modeling methodology of airflow and tracer gas transport in occupied indoor spaces, we established a CFD model based on an experiment conducted by Rim and Novoselac [1]. The experiment was carried out in a controlled environmental chamber equipped with a

thermal manikin, a displacement ventilation diffuser, a tracer gas source, and indoor heat sources (heated boxes and floor). Figure S10 depicts the layout of the chamber and details of the thermal manikin. During the experiment, outdoor air at a controlled temperature (17 ˚C) was continuously supplied using the displacement diffuser with an air change rate of 2.7 h^{-1}. After the airflow was stabilized, a tracer gas (SF_6) was injected at the source position (see Figure S10) for twelve minutes and then the injection was stopped. The SF_6 concentration was monitored for one hour using SF_6 analyzers placed at three locations: (1) room exhaust, (2) 25 cm above the manikin head (S1), and (3) 120 cm above the heated box (S2). The locations of SF_6 analyzers are shown in Figure S11. Additionally, the steady-state vertical profiles of air speeds were measured at three locations (as shown as V1, V2, and V3 in Figure S11). A more detailed description of the experiment can be found in [1].

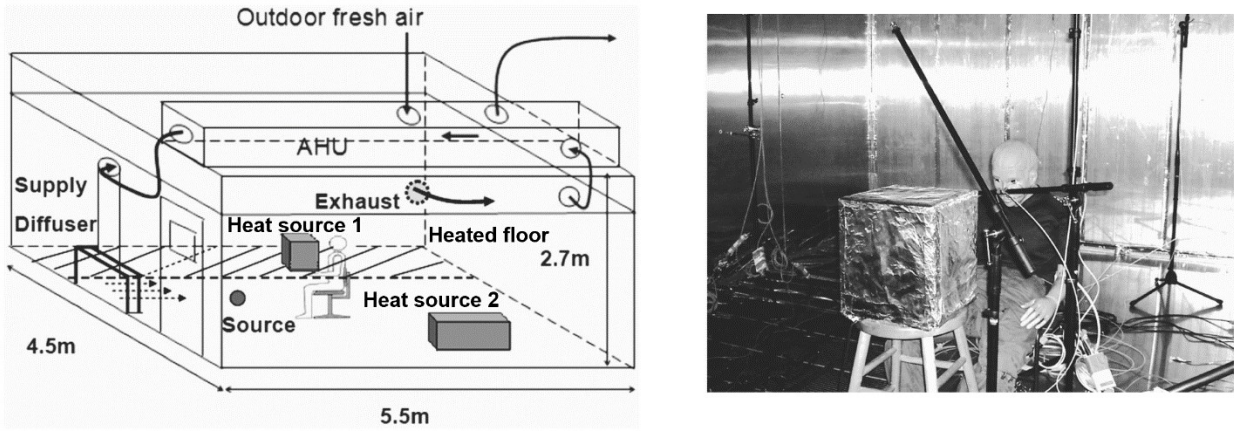

Figure S10. Experimental setup (left) and thermal manikin (right) [1].

Figure S11 presents the geometry of the CFD model developed based on the experiment setup. Note that the modeling strategies were the same as those used in our CFD simulations of classroom, such as turbulence model, tracer gas model, mesh construction, and heat transfer model. A detailed description of the modeling strategies can be found in Section 2 of the main text. Therefore, although the experimental validation had room layout and occupancy that were different from our simulations of classroom, it could provide general insights into the prediction capabilities of our choices of modeling strategies.

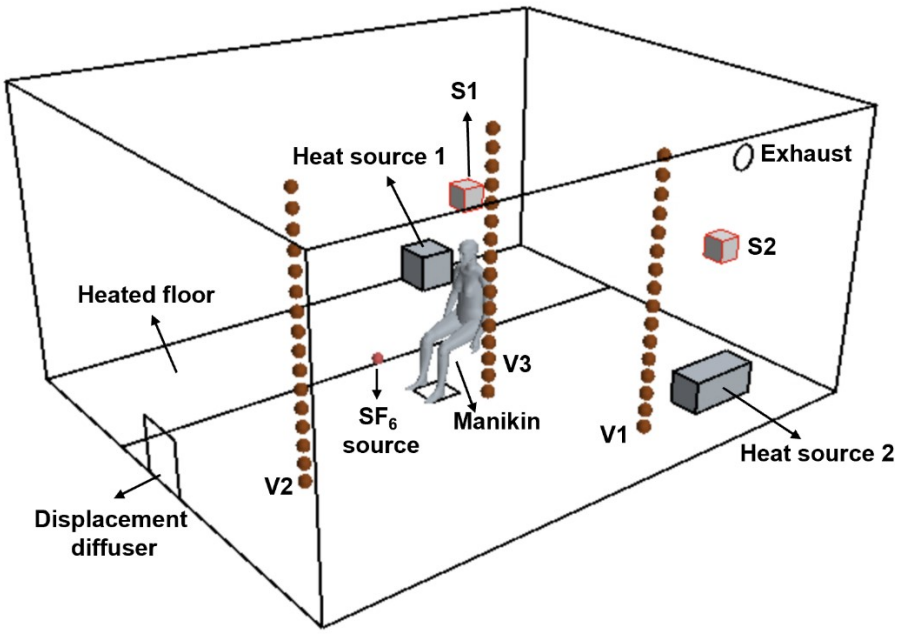

Figure S11. Geometry of CFD model. V1-V3: Measurement locations of vertical profiles of air speeds. S1 and S2: Measurement locations of SF_6 concentrations.

Figure S12 shows the comparisons of simulated vertical profiles of air speeds at three locations against measurements. At locations V1 and V2, air speed was the highest (~0.1 m/s) at the height of 0.1 m, due to the momentum of supplied air at the floor level. At V3 (near the occupant), air speeds were relatively high (>0.12 m/s) at the heights of 0.75 m and 1.70 m, mainly due to the buoyancy-driven thermal plumes around the human body. The simulation results could generally capture these main features of airflow with a Mean Absolute Error (MAE) as 0.022 m/s, which was close to the reported sensor errors (~0.02 m/s). Figure S13 presents the validation results of time-varying SF_6 concentrations. At the room exhaust and sampling locations S1 (above the human head), the simulation could provide reasonable predictions of peak concentrations (with 10.4 % and 9.5 % difference, respectively) and the general trends of temporal concentration variations. Relatively large discrepancies were observed at sampling locations S2, likely because that S2 was close to the room exhaust and there was high concentration gradient. In fact, two previous studies that used the same experiment for CFD validation also reported a notably lower simulated concentrations than measurements at S2 [1,2]. Overall, these validation results suggest that our CFD modeling strategies were able to provide general insights into the airflow and tracer gas transport in occupied, ventilated indoor spaces.

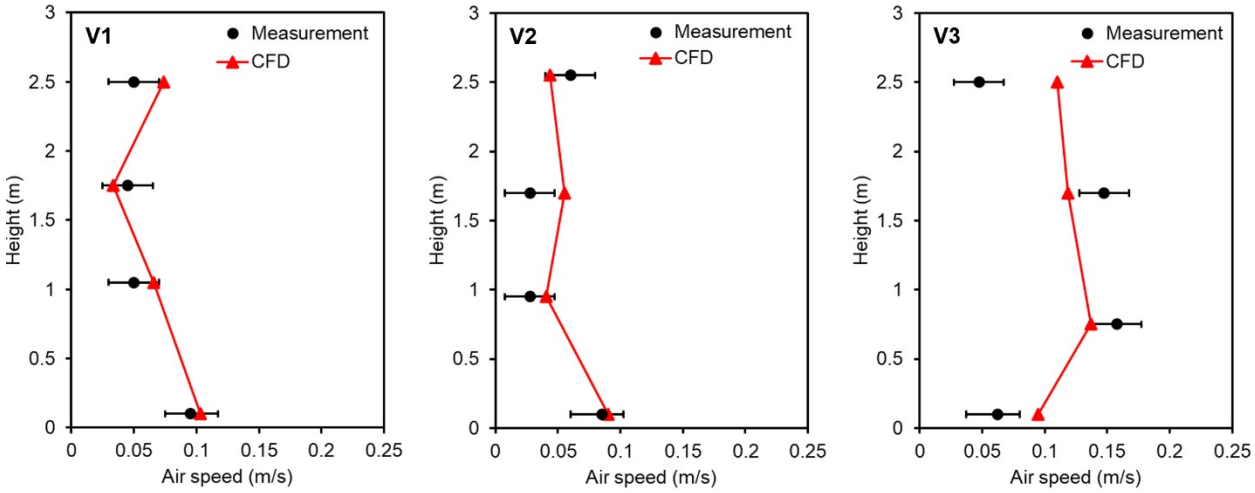

Figure S12. Measured and simulated vertical profiles of air speeds at three locations (V1-V3, see Figure S11).

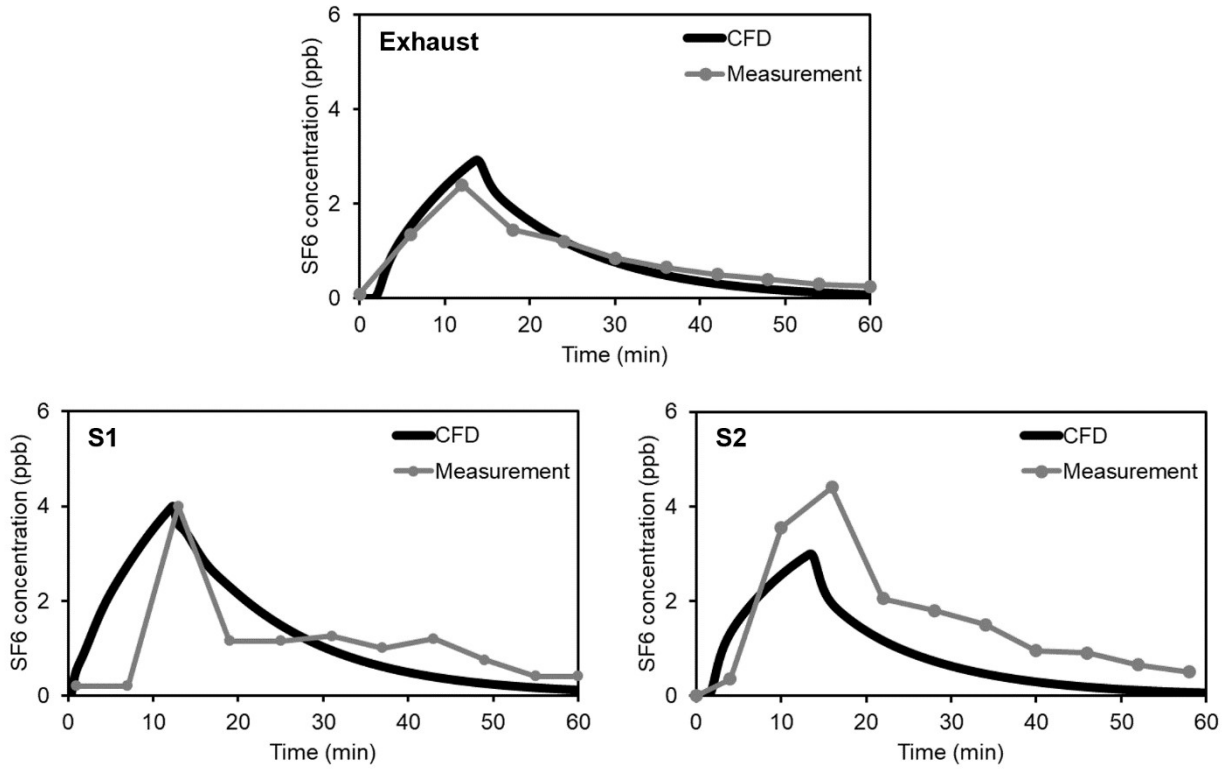

Figure S13. Measured and simulated time-varying SF_6 concentrations at three locations (room exhaust, S1, and S2, see Figure S11).

Reference

1. Rim, D., & Novoselac, A. (2008). Transient simulation of airflow and pollutant dispersion under mixing flow and buoyancy driven flow regimes in residential buildings. *Ashrae Transactions*, *114*, 130.

2. Eom, Y. S., & Rim, D. (2024). Quality control of Lagrangian indoor particle transport simulation: Effects of particle numbers, ventilation strategy, and sampling volume. *Journal of Aerosol Science*, 106346. https://doi.org/10.1016/j.jaerosci.2024.106346